PCCP

Valley ridge inflection points on the potential energy surfaces of H_2S, H_2Se and H_2CO†

Wolfgang Quapp* and Vladlen Melnikov‡

Mathematisches Institut, Universität Leipzig, Augustus-Platz, D-04109 Leipzig, Germany.
E-mail: quapp@rz.uni-leipzig.de

Received 5th March 2001, Accepted 10th May 2001
First published as an Advance Article on the web 14th June 2001

The MP2/6-31G** potential energy surfaces (PES) of the hydrogen sulfide molecule and of the formaldehyde molecule, as well as the MP2/3-21G** PES of the hydrogen selenide molecule are used as qualitative models to locate curves of valley ridge inflection (VRI) points. Crossing points between VRI curves, or VRI manifolds, and approximations of the reaction path allow the identification of a symmetric bifurcation of an assumed reaction path. The recently proposed method of following the reduced gradient is used to calculate reaction path approximations together with their possible bifurcations. The VRI points are calculated with the help of Branin's method, the desingularized global Newton method. The results achieved for the three-atom H_2S and H_2Se are further extended to the four-atom formaldehyde molecule, being a six-dimensional problem, where the directions of symmetrical unimolecular isomerization and dissociation are treated. We discuss the significance of VRI curves.

1 Introduction

The branching of reaction paths is a frequently discussed event in chemistry, but the calculation of branching points still remains a challenge for theoretical chemistry. We seek to understand branching in terms of the PES, which also forms the basis for the conventional transition state theory.[1] Branching of a reaction path leads to the formation of alternative reaction channels on the PES describing the chemical reaction. Some aspects of the bifurcation have already been discussed in earlier publications.[2–4] The methods of the PES analysis[5–7] form the tool to identify the branching of the reaction path. Furthermore, the choice of the path definition is important. The reaction path is an assumed curve in the configuration space of the PES connecting the reactant with one or more products passing the corresponding saddle point (SP) along the so-called minimum energy path (MEP). This way, the MEP is the leading line characterizing the reaction channel in which the trajectories, or, in terms of quantum mechanics, the wave packets should move.[8] However, the term MEP is not yet sufficiently specified to determine a curve uniquely for the reaction path. There are several possibilities to define a reaction path mathematically. The most important definitions are either the steepest descent from the saddle or the gradient extremal, which follows the least ascent.[9] Pathways corresponding to different definitions usually branch at different points of the configuration space.

On the other hand, the PES shows points, which we intuitively connect with the branching of the reaction path, but which do not depend on a reaction path definition. They are defined by the characteristics of the PES itself. Such points are the VRI points.[10–12] The traditional definition is that a VRI point is that point in the configuration space where, orthogonally to the gradient, at least one main curvature of the PES becomes zero. We differentiate between two kinds of points: branching points of diverse path definitions, or VRI points. The ability to reliably calculate the VRI region would provide insight into the stability of vibrational modes and the bifurcation of reaction paths.

As already reported,[13] the VRI points may form a manifold in the configuration space of the molecule. This manifold can have the dimension $N-2$, if the configuration space of the PES has the dimension N.[14,15] At the VRI points, we have 2 constraints: (i) the gradient of the PES has to be orthogonal to an eigenvector of the Hessian matrix of the PES, and (ii) the corresponding eigenvalue has to be zero. Thus, we lose two degrees of freedom for the VRI manifold. Hence, in order to find such manifolds, test surfaces with a dimension higher than $N=2$ are needed. In ref. 11 and 13 we have discussed hypersurfaces over the 3-dimensional configuration space. Now we turn to the PESs of the real molecules H_2S, H_2Se and H_2CO where the latter has an internal dimension of $N=6$ degrees of freedom. The corresponding MP2 *ab initio* PES is used to show the existence, the characteristics and the possible importance of VRI points for locating branching points along possible reaction channels. A one-dimensional manifold of VRI points is found in the case of the 3-atom examples, however, in the case of H_2CO, the manifolds of VRI points are found to be at least two-dimensional. It is obvious that the level of the quantum chemical method used is not sufficient to obtain a globally correct surface of the molecules. Especially, dissociations like $H_2S \rightarrow S + H_2$ cannot be described adequately without using CASSCF or related methods. It is not the objective of this paper to result in an exact description of the high-energy parts of the PES. However, the methods used should be qualitatively correct in the interesting region of the VRI points.

This paper is subdivided as follows: First we repeat the so-called global Newton method, or the Branin method. After that characteristics of VRI points generated by this method will be examined and the manifold of VRI points of the PES

† Electronic Supplementary Information available. See http://www.rsc.org/suppdata/cp/b1/b102053f/

‡ Permanent address: Laboratory of Molecular Spectroscopy, Physics Department, Tomsk State University, Tomsk 634050, Russia.

of H_2S, H_2Se and H_2CO will be specified. The possible significance of those curves or hypersurfaces and of certain points on them is discussed.

2 Reduced gradient curves and their branching points

The idea to follow a reduced gradient has been introduced in ref. 13 and 16. The "reduction" is realized by a projection of the gradient onto the $(N-1)$-dimensional subspace which is orthogonal to the one-dimensional subspace spanned by the search direction $\boldsymbol{r}$. A curve belongs to the search direction $\boldsymbol{r}$, if the gradient of the surface, $\boldsymbol{g}$, always remains parallel to the direction of $\boldsymbol{r}$ at every point along the curve $\boldsymbol{x}(t)$

$$\boldsymbol{P}_r \boldsymbol{g}(\boldsymbol{x}(t)) = 0, \tag{1}$$

where $\boldsymbol{P}_r$ projects with the search direction $\boldsymbol{r}$. This means $\boldsymbol{P}_r \boldsymbol{r} = 0$. Based on the explicit definition, we can follow this curve along its tangential vector. This is the reduced gradient following (RGF) method. In contrast to the conventional distinguished coordinate method (*cf.* ref. 17), a reduced gradient curve passes possible turning points without jumps.[18]

There are two different methods to get a reduced gradient curve: the RGF method and the Branin method.[19] These methods are based on several ideas and have different applications in the examination of the PES. The method of RGF is described in ref. 13 and 16. RGF uses the derivation of eqn. (1) to obtain the tangent $\boldsymbol{x}'$ to the curve

$$\boldsymbol{P}_r \boldsymbol{H} x' = 0. \tag{2}$$

The matrix $\boldsymbol{H}$ is the Hessian. The projector $\boldsymbol{P}_r$ does not depend on the coordinates $\boldsymbol{x}$ or on the curve parameter. In general, the search direction, $\boldsymbol{r}$, and the tangent, $\boldsymbol{x}'$, are different. The algorithm is realized by the predictor-corrector method.[13,20] It is appropriate to detect unknown stationary points, for instance saddle points of index one (transition states). The method starts at a stationary point, *e.g.* a minimum, and follows an arbitrarily selected direction of the gradient on the PES. This may be a chemically interesting direction, a reaction path.

Because the gradient directions of the PES are uniquely determined, curves calculated by RGF to different directions cross if and only if the gradient vanishes at the crosspoint, *i.e.* the crosspoint has to be a stationary point. However, different branches of the solution of the *same* reduced gradient curve may also cross each other. These points are characterized as the branching points of the reduced gradient curve, being the VRI points of the surface. Whenever a reduced gradient curve reaches a VRI point, the curve branches, and at every VRI point of the PES the solution of a reduced gradient curve branches.[13] The characteristic attribute of a VRI point is the zero eigenvalue of the Hessian. At least one eigenvalue changes its sign when going along the gradient,[10,12] where the corresponding eigenvector is orthogonal to the gradient. This means, a valley changes into a ridge or *vice versa.*

The RGF method is related to the well-known mathematically theory of Branin,[19] the so-called global Newton method.[14] Its application to the PES analysis has been described in ref. 13. The procedure uses the adjoint $\boldsymbol{A}$ of the Hessian $\boldsymbol{H}$. It is defined by the equation $\boldsymbol{AH} = \mathrm{Det}(\boldsymbol{H})\boldsymbol{I}$, where $\boldsymbol{I}$ is the unit matrix and $\mathrm{Det}(\boldsymbol{H})$ is the determinant of $\boldsymbol{H}$. The global Newton method defines an autonomous system of differential equations for the curve $\boldsymbol{x}(t)$, where t is a curve length parameter:

$$\boldsymbol{x}' = \mp \boldsymbol{A}(x)\boldsymbol{g}(x), \tag{3}$$

applied as

$$\boldsymbol{x}_{m+1} = \boldsymbol{x}_m \mp \Delta t \boldsymbol{A}(\boldsymbol{x}_m)\boldsymbol{g}(\boldsymbol{x}_m).$$

The sign in eqn. (3) determines the index of the stationary point which we search for. The negative sign stands for stationary points of an even index, *i.e.* minima or second-order SPs. The positive sign stands for stationary points of an odd index, among them SPs of index one (transition structures). The step length of the Branin method depends on the adjoint of the Hessian, $\boldsymbol{A}$, and the gradient, $\boldsymbol{g}$. If the product of adjoint and gradient becomes a zero-vector, the step length becomes also zero. This happens either near stationary points, where the gradient vanishes, or at VRI points. In the second case the determinant of the adjoint of the Hessian vanishes. Hence, stationary points and VRI points are the limits of the Branin method. In mathematical terms, the VRI points are singular points of the Branin method.[14]

The starting point for the Branin method may be any point of the PES, except stationary points or VRI points, whereas the search direction is the gradient. If the search direction of a Branin curve does not exactly coincide with the direction of the gradient at the next VRI point (which we search for), then the curve does not meet this VRI point. A curve is followed where a turning point occurs in front of the VRI, and we cannot grasp the VRI point going along the solution of eqn. (3).[13] Hence, we have to start at a point where the gradient has the same direction as the gradient at the VRI point, see the example of such a search direction in ref. 13. This can be realized for manifolds of VRI points in symmetric subspaces of the configuration space. Therefore, a systematic search for VRI points is possible in symmetry hyperplanes of the PES. In this case, along the pathway of a Branin curve, the eigenvalue of an eigenvector, being orthogonal to the gradient, converges to zero.

3 The potential energy surface of H_2S

Topography and reaction channels

Fits of the PES of H_2S have been reported.[21] The fits are only well adapted to the region of the minimum. However, we use the MP2/6-31G** method of the Gamess-UK program package[22] for the calculations on the PES of the H_2S molecule in a more extended region. Internal mass-weighted coordinates were used, where r denotes the symmetrical distances S–H and α the angle H–S–H. Since the complete 3-dimensional potential energy hypersurface of H_2S cannot be visualized, we use a section for the visualization: the symmetric plane ($r_1 = r_2$, α). The sectional submanifold of the PES is a 2-dimensional surface calculated by single-point MP2 calculations over grids of 41×41 points in the configuration space. Interpolations are done by Mathematica.[23]

Fig. 1 shows the symmetric section of the PES of H_2S. The global minimum is signed with MIN (MP2/6-31G**: $r = 1.327$ Å and $\alpha = 94.37°$, $E = -398.820\,966\,76\ E_h$). The level lines differ by $\Delta E = 0.01\ E_h$. The SP of inversion is at $\alpha = 180°$ at the upper part. The reaction valley related to the dissociation channel symmetrically forming $S + H_2$ can be seen at the bottom on the right-hand side. (Note that a MP2 level calculation is not able to represent the whole dissociation process sufficiently. Note also, that the representation of the H_2S PES in the figure is in curvilinear coordinates, thus, it is distorted.)

The set of valley-ridge-inflection points on the PES of H_2S

In ref. 13 a test surface is used to show that VRI points may form a manifold in the full configuration space. To find this manifold, we constrain the search to a symmetry subspace. The symmetry constraint used is $r_1 = r_2$. In this plane we have automatically realized that the gradient of the full PES is orthogonal to the eigenvector of the antisymmetric stretch mode which stands orthogonal on the plane $r_1 = r_2$. This third dimension of the antisymmetric stretch mode of the con-

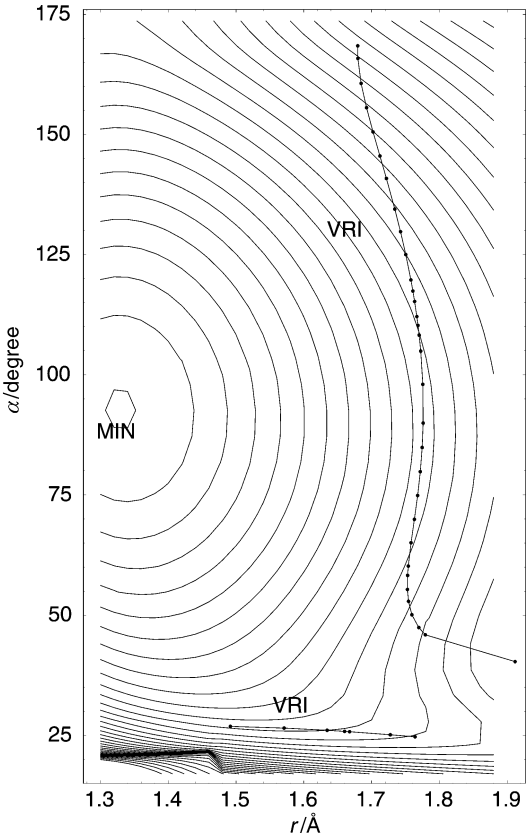

Fig. 1 (r_{sym}, α)-section of the PES of H_2S (MP2/6-31G**). MIN is the global minimum. Level lines begin at -398.8205 E_h with a spacing of 0.01 E_h. The VRI manifolds are two curves depicted by VRI.

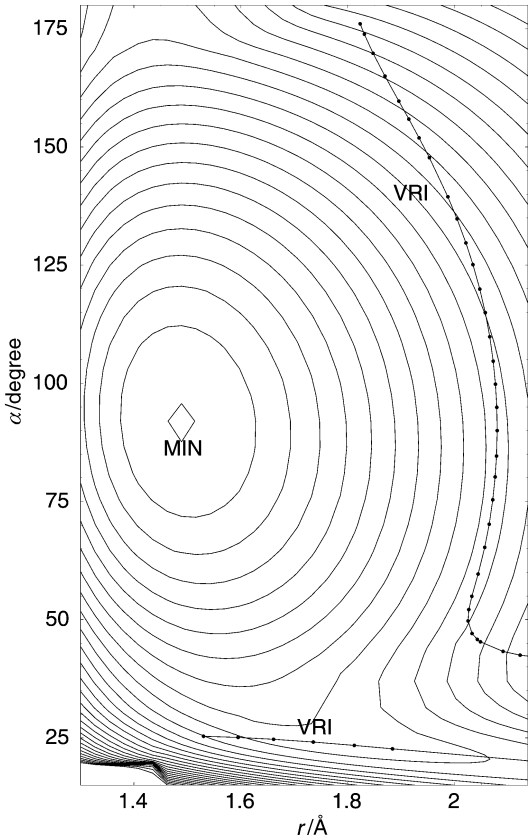

Fig. 2 (r_{sym}, α)-section of the PES of H_2Se (MP2/3-21G**). MIN is the global minimum. Level lines begin at -2389.6790 E_h with a spacing of 0.01 E_h. The VRI manifolds are two curves depicted by VRI.

figuration space is not shown in Fig. 1. The first condition (i) for a VRI point is automatically fulfilled in the symmetric plane. The search for a VRI point has to look for condition (ii) only, the zero eigenvalue of the antisymmetric mode. Using the Branin method, it is possible to search systematically for VRI points of the PES of symmetric configurations of H_2S. The resulting curves of VRI points of the PES of H_2S are shown in Fig. 1. The curves "VRI" are two distinct manifolds of VRI points. The method of calculation is an interactive point by point calculation, and it can be described as follows: In order to find a point, we first fix a starting point. After convergence of the Branin method eqn. (3) to a VRI point, the next initial point is selected, for example by changing the angle coordinate of the upper VRI curve by 5°. Again, we look for convergence. The used convergence criterion is an eigenvalue of wavenumber <1 cm^{-1}. The sign used in the Branin search depends on the side of the VRI curve where the initial point is located (relative to the global minimum MIN). If necessary, we have to restart the procedure with the opposite sign. The calculated points are also listed in Table 1 of the supplementary data.† The visualization of bifurcating curves of an assumed minimum energy path at the corresponding VRI point is outlined in ref. 11. There the water molecule has been used, but here the relations are analogous.

4 The PES and VRI points of H_2Se

There are known PES fits.[24] We use the MP2/3-21G** method of the Gamess-UK program package[22] for the calculations on the H_2Se molecule, because the fits are only well adapted to the region of the minimum. Internal mass-weighted coordinates have been used, where r denotes the symmetric distances Se–H and α the angle H–Se–H. We use the analogous visualization to the case of H_2S. Again, the section is the symmetric plane ($r_1 = r_2$, α). Fig. 2 shows the symmetric section of the PES of H_2Se. The sectional submanifold of the PES is a 2-dimensional surface calculated by single-point MP2/3-21G** calculations over grids of 41×41 points in the configuration space. Interpolations are done by Mathematica.[23] The global minimum is signed with MIN (MP2/3-21G**: $r = 1.4883$ Å, $\alpha = 92.277°$, $E = -2389.679\,419\,61$ E_h). Again, the SP of inversion is at $\alpha = 180°$. The region of a reaction valley related to the dissociation channel forming $Se + H_2$ is in the lower right corner of the figure. (Note that the MP2 level of the calculation is not able to represent the whole dissociation process sufficiently.) Using the Branin method, we calculate the VRI points of the PES of symmetric configurations of H_2Se. The resulting curves of VRI points of the PES of H_2Se are shown by the curves "VRI" and are reported in Table 2 of the supplementary data.†

5 The potential energy surface of H_2CO

We use the MP2/6-31G** method of the Gamess-UK program package[22] for the calculations of the H_2CO molecule.

Visualization by cross sections

The dimension of internal coordinates for the description of H_2CO is $N = 6$. We use distances to the C atom: r_1 and r_2 are the distances between the H_1/H_2 and C, and r_3, correspondingly, is the distance O–C. The angles H–C–O are α_1 and α_2, thus, correspondingly, the angle H–C–H is (in plane) $\beta = 2\pi - \alpha_1 - \alpha_2$. The out-of-plane angle of the H_1–C–O plane to the plane of the atoms H_2–C–O is δ. It is the "book mode" angle of the molecule. As in the previous cases, we are interested in the VRI points of the bowl of the global minimum at $r_3 = 1.219$ Å, $r_1 = r_2 = 1.099$ Å, $\alpha_1 = \alpha_2 =$

122.23° with an energy of $E = -114.191\,015\,72\ E_h$. The complementary angle $\beta = \beta_{sym}$ is 115.54°. The first section used for visualization is the (r_1, r_2) plane for fixed $\alpha_1 = \alpha_2 = 122.23°$ where again $\delta = 180°$ is fixed, as well as r_3 which is fixed at the value of $r_3 = 1.322$ Å, see Fig. 3. The next sections for several further possibilities of visualization are symmetry planes with $R = R_{sym} = r_1 = r_2$, $\beta = \beta_{sym} = 360° - 2\alpha$, where $\alpha_1 = \alpha_2$, and fixed $\delta = 180°$. These conditions are three symmetry constraints. Finally there is the CO distance r_3. For Fig. 4, the CO distance r_3 is optimized, point by point over a 43 × 43 raster, as is often done in quantum chemistry. For Fig. 5, r_3 is fixed to the equilibrium length of the minimum, 1.219 Å, but for Fig. 6, we use the fixed distance of $r_3 = 1.460$ Å. These sectional submanifolds of the PES with fixed r_3 give 2-dimensional surfaces calculated by single-point MP2/6-31G** calculations over grids of 43 × 85 points in the configuration space. Interpolations are done by Mathematica.[23]

In Fig. 4 we draw thick lines for the equipotential lines of the PES, but thin lines for the optimized values of the r_3 distance which changes noticeably. Note: at the right upper corner of Fig. 4, and still more at the right lower corner, drawbacks of the MP2 perturbation procedure emerge: it jumps between two very different values of r_3. The result is a strange "saddle point" region. A site of fracture is seen, and the "valley of the SP" has an edge at the side of the dissociation to H_2 + CO. The MP2 method used does not work correctly (*cf.* ref. 25 and 26) at this site of fracture at the transition to shorter r_{CO} values. The symmetry constraind "SP" of Fig. 4 may be in the region of $R_{sym} \approx 1.5$ Å, $\beta_{sym} \approx 43°$, and at an energy of $\approx -113.94\ E_h$. This SP of higher index is not of practical interest.

Fig. 3 shows one single VRI point at the fixed $\alpha_1 = \alpha_2$, and fixed r_3 in the plane of the two different H–C distances. This suggests that the normal modes of stretching, ν_1 and ν_5, of the two H atoms could become unstable at the VRI region, *cf.* Table 1 and Fig. 7 for the normal modes of H_2CO.[27,28] The VRI point is obtainable if we start at the minimum and if we go uphill exactly along the symmetry axis $r_1 = r_2$. This also is the way to calculate the VRI points of the next figures: we hold the symmetry exactly, but it is possible to change the relation between the distances $R = r_1 = r_2$ and $\beta = 2\pi - \alpha_1 - \alpha_2$ where the angles $\alpha_1 = \alpha_2$. (The calculated VRI points of Fig. 6 are listed in Table 3 of the supplementary data.†) Under the given symmetry constraints we obtain that the gradient is orthogonal to the three out-of-symmetry modes, the antisymmetric stretch, the antisymmetric bend and the out-of-plane mode. The Branin method has to search "only" for the zero eigenvalues of those modes, to localize their VRI points. In comparison to the former H_2X molecules, we have an additional out-of-plane mode ν_4 in this 4-atom molecule (curve VRI_3), and a second antisymmetric mode, the antisymmetric bending ν_6. However, the "inner" VRI_1 curve is quite similar to those of the former 3-atom molecules. The reason may be that the symmetry constraint of two equal angles forces the "diatom" part, CO, of the molecule to act as a single entity, from the point of view of the two symmetric H atoms.

But now, an additional characteristics emerges: the bifurcation of the corresponding RGF curves at the corresponding VRI points from the plane of Fig. 5 or 6 can take place along 3 degrees of freedom, into 3 different antisymmetric directions,

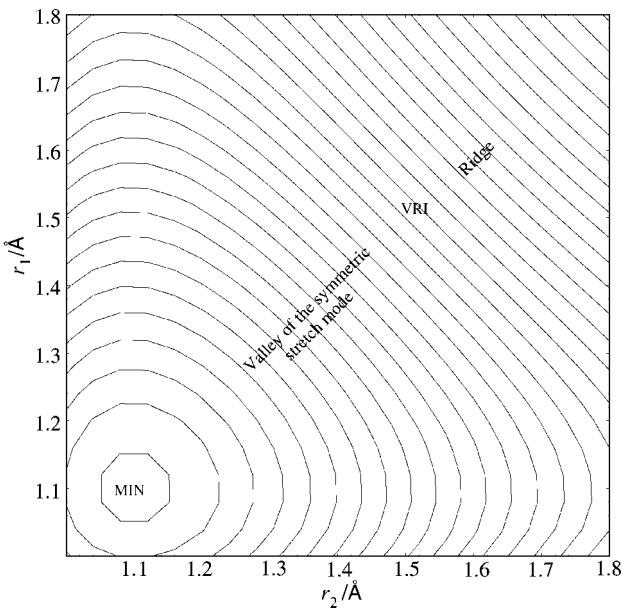

Fig. 3 (r_1, r_2)-section of the PES of H_2CO (MP2/6-31G**). MIN is the minimum of the section. The VRI point is near $r_1 = r_2 \approx 1.57$ Å. The CO distance r_3 is fixed at 1.322 Å.

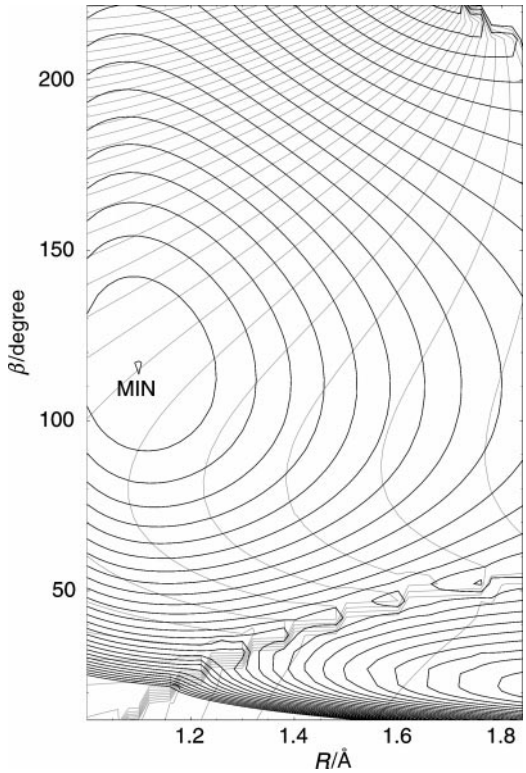

Fig. 4 (R_{sym}, β_{sym})-section of the PES of H_2CO (MP2/6-31G**). The level lines begin at $-114.1909\ E_h$ with a spacing of $0.02\ E_h$. MIN is the global minimum. The CO distance r_3 is optimized at every point of the 43 × 43 point raster. The system of r_3 level lines is underlined in gray tone under the PES level lines which are drawn as usual bold lines. The levels of r_3 begin at 1.159 Å at the lower corner of the right hand side, and they have a spacing of 0.010 Å. (Note: at the right corners, the MP2 procedure "jumps".)

Table 1 Fundamental transition wavenumbers, symmetries, and motions for H_2CO[a]

Normal mode	Wavenumber /cm^{-1}	Approximate motion
$\nu_1(A_1)$	2944[b]	Symmetric C–H stretch
$\nu_2(A_1)$	1764	C=O stretch
$\nu_3(A_1)$	1563	CH_2 bend
$\nu_4(B_1)$	1191	out-of-plane bend
$\nu_5(B_2)$	3009	antisymmetric C–H stretch
$\nu_6(B_2)$	1287	CH_2 rock mode

[a] See Fig. 7 for illustration of the normal mode motion. [b] Ref. 27 and 28.

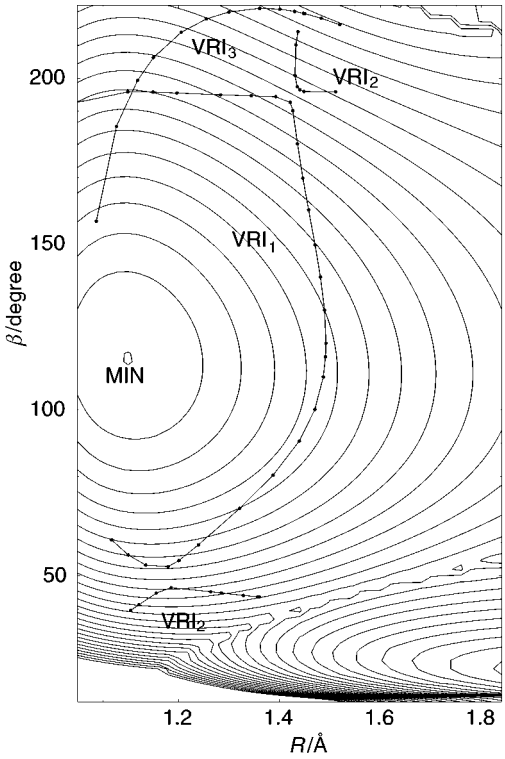

Fig. 5 (R_{sym}, β_{sym})-section of the PES of H_2CO (MP2/6-31G**). The level lines begin at -114.1909 E_h with a spacing of 0.02 E_h. The CO distance r_3 is fixed at 1.219 Å, the equilibrium distance of the global minimum MIN. By the dotted special curves we draw the calculated VRI points. The section of the first VRI manifold with this PES section is depicted by curve VRI_1. Correspondingly, the next VRI points form the manifolds VRI_2 and VRI_3. The latter are the bifurcations of the out-of-plane mode.

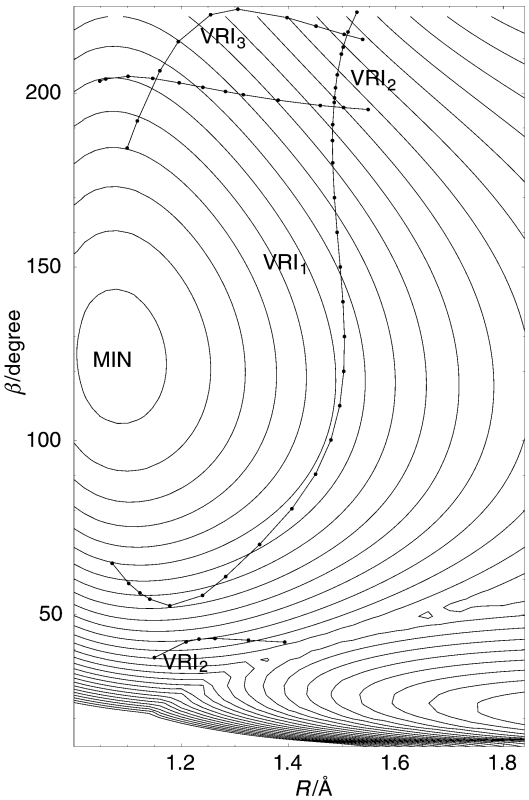

Fig. 6 (R_{sym}, β_{sym})-section of the PES of H_2CO (MP2/6-31G**). The level lines begin at -114.1309 E_h with a spacing of 0.02 E_h. The CO distance r_3 is fixed at 1.460 Å. MIN is the (shifted) minimum of this section. By the dotted special curves we draw the calculated VRI points. VRI_3 points are the bifurcation points of the out-of-plane mode. Analogous curves are obtained for other r_3 distances of the CO diatom.

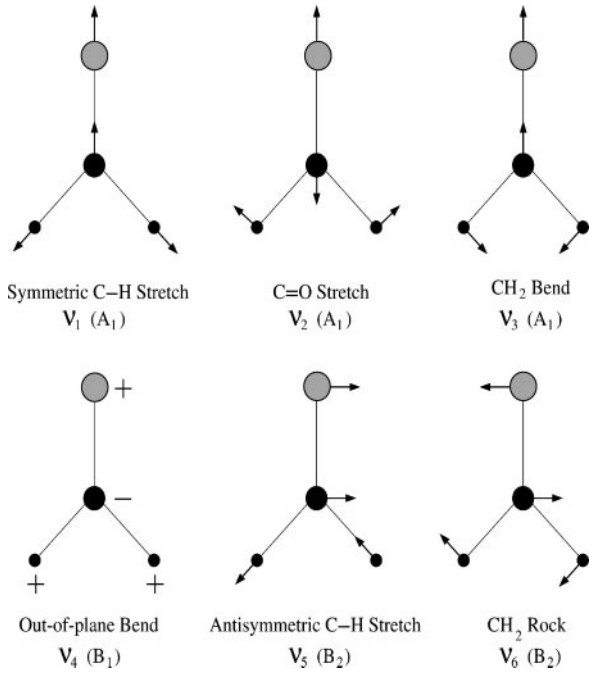

Fig. 7 Six normal vibrational modes of formaldehyde, H_2CO, *cf.* ref. 27.

the antisymmetric C–H stretch (ν_5 at the minimum) as in the 3-atom molecules, or the antisymmetric CH_2 rock mode (ν_6 at the minimum) (both of B_2 symmetry), or the out-of-plane bend mode (ν_4 at the minimum) of B_1 symmetry. Because there are 3 different degrees of freedom for an antisymmetric bifurcation, we find 3 VRI curves in Fig. 5 and 6 depicted by VRI_1, VRI_2 and VRI_3. Note: the corresponding zero eigenvectors point out of the plane of Fig. 5 and 6.

The VRI_3 describes the bifurcation from the symmetry plane into symmetry B_1, where the other two curves are connected by the same symmetry B_2. So, two of these possibilities have the same symmetry, B_2, and can mix. Consequently, we find a combination of both directions as the result of our calculations for the eigenvector which belongs to the zero frequency at the corresponding VRI point. This is shown schematically in Fig. 8 for the case $r_3 = 1.219$ Å, *i.e.* for the B_2-VRI curves of Fig. 5. We use the calculated eigenvectors for the zero eigenvalue at the VRI_1 and VRI_2 curves which belong to the atom H_1. The plane (r_1, $\beta_1 = 180° - \alpha_1$) of the H_1 atom alone is shown, the VRI curves VRI_1 and VRI_2 of the foot-points of the zero eigenvectors of B_2 symmetry being the same curves as in Fig. 5. Only the projection of the eigenvectors into the (r_1, β_1)-plane is used; note also that the r_3 component (the CO part) has usually a small, but nonzero component in these eigenvectors, but the component of the out-of-plane mode ν_4 is always zero. The orientation of the vectors is selected in such a way that for VRI_1 the stretching of r_1 is chosen negative, and the corresponding β_1 is used. Of course, an analogous description of the H_2 atom with r_2 and β_2 would start at the same curves VRI_1, VRI_2 and lead to similar, but complementarily directed vectors.

It comes out that at the pathway into the symmetric stretch mode of the C–H bonds ν_1, in Fig. 5 in a horizontal direction starting at the minimum, the VRI eigenvector is mainly the antisymmetric stretch ν_5, see Fig. 8. Whereas starting at the pathway into the normal mode direction of the symmetric angle mode ν_3 (in Fig. 5 the vertical direction starting at the minimum, the CH_2 bend) causes the VRI eigenvector to be mainly the antisymmetric rock ν_6. Of special interest are the two regions where the VRI curves 1 and 2 are in close contact: these contact areas are at 1.18 Å and $\beta_{sym} = 50°$, and at 1.43 Å and $\beta_{sym} = 195°$. If the two VRI curves 1 and 2

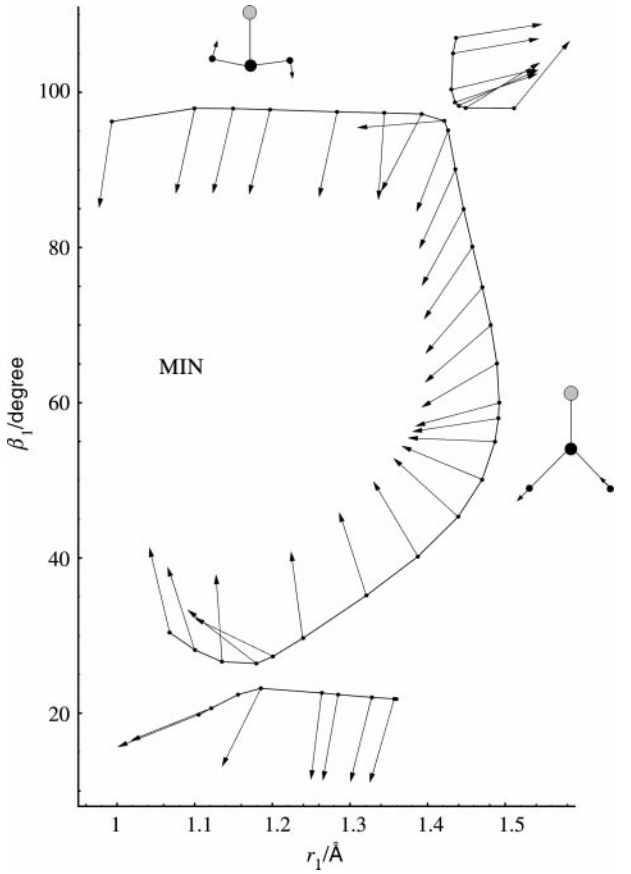

Fig. 8 The eigenvectors to the zero eigenvalue at the curves VRI_1 and VRI_2 of Fig. 5 which act at the atom H_1. Only the projection into the antisymmetric direction (r_1, β_1) is shown. The length of the vectors is normalized. The equivalent vectors of H_2 along direction ($-r_2$, $-\beta_2$) and the direction of the distance change of r_3 are not shown.

cross, their zero eigenvalues degenerate! The calculation of eigenvectors becomes non-unique, and this can be seen in Fig. 8: the eigenvectors near the two crossing points become erratic.

The out-of-plane degree of freedom can also serve for the bifurcation direction. This is curve VRI_3. Of course, for the VRI point to have a chemical meaning, the first emergence of a VRI point is of particular interest if seen from the minimum. The second or the third curve of VRI points seen from the minimum depict VRI points of higher index. There, the dimension of the ridge is two or more. Already the first VRI point causes an instability of the mode which crosses its VRI point curve and will cause a bifurcation of the corresponding reaction channel. Thus, as we know from the discussion of saddle points,[29] those points of higher index are not so interesting as the corresponding points of index one.

The r_3 problem. The VRI curves in Fig. 5 and 6 are calculated with constant $r_3 = 1.219$, or 1.460 Å, respectively. In contrast, for the "PES-part" of Fig. 4 we have optimized the C–O distance, r_3, at every raster point. (The result is depicted by the gray underlying equidistance levels of r_3.) The PESs of Fig. 5 and 6 are not very different. If we use other values of r_3 for the calculation of the VRI curves, in other PES sections, then we get only slightly different VRI curves. This means that if we connect corresponding curves of different r_3 values, we obtain at least 2-dimensional surfaces of VRI points in the 3-dimensional space of the symmetry coordinates R_{sym}, β_{sym} and r_3, which are embedded in the 6 dimensions of the full configuration space. For every antisymmetric mode we have one surface of VRI points. It is also possible that these surfaces intersect, as is the case for $r_3 = 1.460$ Å for the two modes of B_2 symmetry, or for the surfaces of VRI_1 and VRI_3 of different symmetry. At the intersection we find a degeneracy of the zero eigenvalue.

6 Discussion

We find curves of VRI points, *i.e.* one-dimensional manifolds, for H_2S and H_2Se, as well as three different, at least 2-dimensional manifolds of VRI points in the case of H_2CO. (Note that the results of H_2CO are only obtained for VRI points in symmetry subspaces.) The results revise the older view of the problem,[30] which suggested to obtain an isolated, well-defined VRI point. The method of following a reduced gradient (RGF)[16] as well as the Branin method[13] have succeeded in computing the VRI points.

The results reported in this paper raise the question of the significance of high-dimensional manifolds of VRI points. Which points on the VRI manifold correspond to the chemical concept of reaction path branching? To answer this question we need a criterion allowing us to decide whether a VRI point is located on a MEP or not. The IRC is not defined locally and so it is unsuitable for such a task. In contrast, if a VRI point fulfills the conditions of a gradient extremal[31] and the eigenvalues of the Hessian indicate a valley, this VRI point is located on a MEP and so this VRI point is the branching point of that reaction path.

Now we consider the reaction path which follows the symmetric H_2 + S dissociation of H_2S, or the symmetric H_2 + Se dissociation of H_2Se, or the symmetric H_2 + CO dissociation of H_2CO. In fact, a gradient extremal for H_2S crosses the VRI curve near the point at $r = 1.76$ Å, $\alpha = 24.7°$ in Fig. 1, and for H_2Se at $r = 1.88$ Å, $\alpha = 22.7°$ in Fig. 2. (We have used a gradient extremal program of Imig and Quapp, University Leipzig, 1996. The VRI points nearby are marked in Tables 1 to 3 of the supplementary data.†) The unimolecular dissociation $H_2CO \rightarrow H_2 + CO$ is Woodward–Hoffmann forbidden therefore proceeds *via* the highly asymmetric saddle point. It is known that the bifurcation of the dissociation path leads to a non-symmetric pathway of that reaction.[26,32] To compare a possible start of that path, we have calculated the full 6-dimensional gradient extremals of H_2CO starting at the global minimum. A gradient extremal (mainly along an increasing CO distance but holding the full symmetry of Fig. 4) leads to the saddle point region of Fig. 4–6, indicating the pathway to H_2 + CO. It crosses a VRI point in the stretching mode region at $R_{sym} = 1.425$ Å, $\beta_{sym} = 81°$, but at the large CO distance of $r_3 = 1.646$ Å. This is far above the section of VRI points in Fig. 6, and it is also far away from the shortening of the CO distance under the dissociation, thus, we cannot discuss the pathway within the results of this VRI calculation.

However, with Fig. 5, we may imagine the $H_2CO \rightarrow H + CO + H$ theoretical reaction path. The gradient extremal of the dissociation path uphill from the symmetric stretching valley crosses VRI_1 at $R_{sym} = 1.485$ Å, $\beta_{sym} = 122°$, and the slightly smaller CO distance of $r_3 = 1.189$ Å, in comparison to the CO distance used in Fig. 5. A bifurcation on this (full 6-dimensional) valley pathway at VRI_1 would lead along an antisymmetric stretch mode, out of the plane of a section like Fig. 5, to the energetically lower paths to one of the saddle points of the pathways to the two HCO + H versions. Behind the VRI_1, the gradient extremal of the symmetric stretch in the plane of a section (like Fig. 5 but at $r_3 = 1.189$ Å) would go further up a ridge (the ridge eigenvector is that of the corresponding orthogonal antisymmetric stretch mode). This dimension is not shown in Fig. 5. An analogous illustration has already been given in ref. 11. This ridge is also a gradient extremal, but it loses the characterization of a reaction pathway. In this way we can state that there is a bifurcation of the reaction path. (Note: the gradient extremal itself

does not bifurcate at the crossing of the VRI line,[31] it only changes its characterization.)

Further gradient extremals also cross VRI points: that of a symmetric bending excitation crosses at $R_{sym} = 1.071$ Å, $\beta_{sym} = 162°$ and at the large $r_3 = 1.632$ Å a VRI_3 point of the out-of-plane book mode, and at $R_{sym} = 1.077$ Å, $\beta_{sym} = 212°$ and $r_3 = 1.496$ Å the anti-symmetric bending mode VRI_1, correspondingly. These two points are again above the calculated upper section of VRI points in Fig. 6. The corresponding gradient extremal slowly follows the valley of Fig. 4 along an increasing β value (the opening of mode ν_3), but r_3 rapidly increases on this pathway (mode ν_2) up to a turning point in the r_3 direction. Thus, the use of the gradient extremal as a reaction path is again questionable, in this case.

Finally, we try to generalize the significance of the curve of VRI points. A set of RGF curves referring to different search directions of the PES can be calculated. Some of the curves cross the VRI manifold and branch there. The directions of their gradients can be compared with combinations of normal modes of the equilibrium structure. The curve of VRI points of the PES may be considered as the outer limit for stable modes in the symmetric subspace, *i.e.* for the combinations of the symmetric stretching modes, ν_1, ν_2, and the symmetric bending, ν_3, *cf.* ref. 11.

Acknowledgements

We thank M. Hirsch for stimulating discussions, and D. Heidrich for reading the manuscript. Our work could only have been carried out through the financial support of the Deutsche Forschungsgemeinschaft. VM thanks the Saxon State Ministry of Science and Art for a stipend.

References

1 K. Laidler, *Theory of Reaction Rates*, McGraw-Hill, New York, 1969.
2 H. Metiu, J. Ross, R. Silbey and T. F. George, *J. Chem. Phys.*, 1974, **61**, 3200.
3 P. Valtazanos and K. Ruedenberg, *Theor. Chim. Acta*, 1986, **69**, 281.
4 W. A. Kraus and A. E. De Pristo, *Theor. Chim. Acta*, 1986, **69**, 309.
5 P. G. Mezey, *Potential Energy Hypersurfaces*, Elsevier, Amsterdam, 1987.
6 D. Heidrich, W. Kliesch and W. Quapp, *Properties of Chemically Interesting Potential Energy Surfaces*, Springer, Berlin, 1991.
7 D. Heidrich, *The Reaction Path in Chemistry: Current Approaches and Perspectives*, Kluwer, Dordrecht, 1995.
8 A. H. Zewail, *J. Phys. Chem.*, 2000, **104**, 5660.
9 D. K. Hoffman, R. S. Nord and K. Ruedenberg, *Theor. Chim. Acta*, 1986, **69**, 265.
10 J. Baker and P. M. W. Gill, *J. Comput. Chem.*, 1988, **9**, 465.
11 M. Hirsch, W. Quapp and D. Heidrich, *Phys. Chem. Chem. Phys.*, 1999, **1**, 5291.
12 W. Quapp, *J. Chem. Phys.*, 2001, **114**, 609, DOI: 10.1063/1.1330237.
13 W. Quapp, M. Hirsch and D. Heidrich, *Theor. Chem. Acc.*, 1998, **100**, 285.
14 H. Th. Jongen, P. Jonker and F. Twilt, in *Parametric Optimization and Related Topics*, ed. J. Guddat, H. Th. Jongen, B. Kummer and F. Nožička, Akademie-Verlag, Berlin, 1987, p. 209.
15 I. Diener, Habilitation, Göttingen, 1991.
16 W. Quapp, M. Hirsch, O. Imig and D. Heidrich, *J. Comput. Chem.*, 1998, **19**, 1087.
17 I. H. Williams and G. M. Maggiora, *J. Mol. Struct.* (*Theochem.*), 1982, **89**, 365.
18 W. Quapp, *J. Comput. Chem.*, 2001, **22**, 537.
19 F. H. Branin, *IBM J. Res. Develop.*, 1972, **16**, 504.
20 E. L. Allgower and K. Georg, *Numerical Continuation Methods—An Introduction*, Springer, Berlin, 1990.
21 (*a*) I. N. Kozin and P. Jensen, *J. Mol. Spectrosc.*, 1994, **163**, 483; (*b*) O. L. Polyansky, P. Jensen and J. Tennyson, *J. Mol. Spectrosc.*, 1996, **178**, 184; (*c*) S. Ding and Y. Zheng, *J. Chem. Phys.*, 1999, **111**, 4466.
22 M. F. Guest, P. Fantucci, R. J. Harrison, J. Kendrick, J. H. van Lenthe, K. Schoeffel and P. Sherwood, *GAMESS-UK Program*, Revision C.0, CFS Ltd., Daresbury Lab, 1993.
23 S. Wolfram, *MATHEMATICA*, Version 3.0, Wolfram Research Inc., Champain, USA, 1997.
24 I. N. Kozin and P. Jensen, *J. Mol. Spectrosc.*, 1993, **160**, 39; I. N. Kozin and P. Jensen, *J. Mol. Spectrosc.*, 1993, **160**, 46.
25 Z. Havlas, T. Kovář and R. Zahradník, *J. Mol. Struct.* (*Theochem.*), 1986, **136**, 239.
26 F. Jensen, *Theor. Chem. Acc.*, 1998, **99**, 295.
27 R. J. Bouwens, J. A. Hammerschmidt, M. M. Grzeskowiak, T. A. Stegink, P. M. Yorba and W. F. Polik, *J. Chem. Phys.*, 1996, **104**, 460.
28 (*a*) K. Yagi, T. Taketsugu, K. Hirao and M. S. Gordon, *J. Chem. Phys.*, 2000, **113**, 1005; (*b*) Y. Y. Yamaguchi, R. B. Remington, J. F. Gaw, H. F. Scharfer and G. Frenking, *Chem. Phys.*, 1994, **180**, 55; (*c*) C. B. Moore and J. C. Weishaar, *Annu. Rev. Phys. Chem.*, 1983, **34**, 525.
29 D. Heidrich and W. Quapp, *Theor. Chim. Acta*, 1986, **70**, 89.
30 (*a*) A. Tachibana, I. Okazaki, M. Koizumi, K. Hore and T. Yamabe, *J. Am. Chem. Soc.*, 1985, **107**, 1190; (*b*) B. J. Smith, D. J. Swanton, J. A. Pople, H. F. Schaefer and L. Radom, *J. Chem. Phys.*, 1990, **92**, 1240; (*c*) R. G. A. Bone, T. W. Rowlands, N. C. Handy and A. J. Stone, *Mol. Phys.*, 1991, **72**, 33; (*d*) R. G. A. Bone, *Chem. Phys. Lett.*, 1992, **193**, 557; (*e*) T. Taketsugu and T. Hirano, *J. Chem. Phys.*, 1993, **99**, 9806; (*f*) R. G. A. Bone, *Chem. Phys.*, 1993, **178**, 255; (*g*) T. Taketsugu and T. Hirano, *J. Mol. Struct.* (*Theochem.*), 1994, **130**, 169; (*h*) J. L. Liao, H. L. Wang and H. W. Xin, *Chin. Sci. Bull.*, 1995, **40**, 566; (*i*) T. Taketsugu and M. S. Gordon, *J. Chem. Phys.*, 1995, **103**, 10042; (*j*) Y. Yanai, T. Taketsugu and T. Hirano, *J. Chem. Phys.*, 1997, **107**, 1137; (*k*) G. V. Shustov and A. Rauk, *J. Org. Chem.*, 1998, **63**, 5413.
31 W. Quapp, M. Hirsch and D. Heidrich, *Theor. Chem. Acc.*, 2000, **105**, 145, DOI 10.1007/s00214990000192.
32 (*a*) X. S. Li, J. M. Millen and H. B. Schlegel, *J. Chem. Phys.*, 2000, **113**, 10062; (*b*) D. Feller, M. Dupois and B. C. Garrett, *J. Chem. Phys.*, 2000, **113**, 218; (*c*) B. J. Sung and M. S. Kim, *J. Chem. Phys.*, 2000, **113**, 3098; (*d*) H. Nakano and K. Hirao, *Chem. Phys. Lett.*, 2000, **317**, 90; (*e*) L. M. M. de A. Martins, G. Arbilla and E. C. de Silva, *J. Phys. Chem.*, 1998, **102**, 10805; (*f*) J.-S. K. Yu and C. Yu, *Chem. Phys. Lett.*, 1997, **271**, 259; (*g*) B. S. Jursic, *J. Mol. Struct.* (*Theochem.*), 1997, **418**, 11; (*h*) L. Deng, T. Ziegler and L. Fan, *J. Chem. Phys.*, 1993, **99**, 3823; (*i*) H.-L. Dai, *Appl. Spectrosc.*, 1990, **44**, 1595; (*j*) G. E. Scuseria and H. F. Schaefer III, *J. Chem. Phys.*, 1989, **90**, 3629.